IOP Publishing Journal of Physics: Condensed Matter
J. Phys.: Condens. Matter **34** (2022) 144002 (8pp) https://doi.org/10.1088/1361-648X/ac4b2b

Non-quantum chirality in a driven Brusselator

Jason A C Gallas *

Instituto de Altos Estudos da Paraíba, Rua Silvino Lopes 419-2502, 58039-190 João Pessoa, Brazil
Complexity Sciences Center, 9225 Collins Avenue Suite 1208, Surfside, FL 33154, United States of America
Max-Planck-Institut für Physik komplexer Systeme, Nöthnitzer Str. 38, 01187 Dresden, Germany

E-mail: jason.gallas@gmail.com

Received 13 November 2021, revised 11 January 2022
Accepted for publication 13 January 2022
Published 31 January 2022

Abstract

We report the discovery of non-quantum chirality in the a periodically driven Brusselator. In contrast to standard chirality from quantum contexts, this novel type of chirality is governed by rate equations, namely by purely classical equations of motion. The Brusselator chirality was found by computing high-resolution phase diagrams depicting the number of spikes, local maxima, observed in stable periodic oscillations of the Brusselator as a function of the frequency and amplitude of the external drive. We also discuss how to experimentally observe non-quantum chirality in generic oscillators governed by nonlinear sets of rate equations.

Keywords: non-quantum, chirality, driven, Brusselator

(Some figures may appear in colour only in the online journal)

1. Background

A recent work reported the observation of chiral structures of non-quantum origin in the dynamics of an autonomous, that is time independent, electronic circuit, Hartley's oscillator, involving a solid-state component, namely a junction-gate field-effect transistor, and a tapped coil [1]. Such remarkable structures were observed in phase diagrams displaying how the number of spikes of stable periodic oscillations changed when parameters of the circuit are tuned along certain closed parameter paths, rings, in the control parameter space of the circuit.

The observation of such chiral structures is significant because the electronic circuit is governed by purely classical (that is, not quantum) equations of motion. As it is well-known, chirality is a familiar property commonly associated with quantum phenomena, in particular with the spatial orientation of the atoms in molecules, the biochemistry of living organisms, and spin properties [2–11]. In other words, the chirality recorded for the electronic circuit is of a radically distinct nature, produced by properties which are not at all associated with quantum phenomena.

So far, there are only two known examples of dynamical systems displaying non-quantum chirality. First, the aforementioned electronic oscillator of Hartley [1]. Second, a photochemically driven ruthenium-catalyzed Belousov–Zhabotinsky reaction model [12]. These two instantiations of non-quantum chirality have a rather distinct physical nature, electronic and physico-chemical. Furthermore, the mathematical nature of equation of motions underlying both phenomena is also conspicuously different: the electronic circuit is governed by an autonomous equations while the chemical reaction model involves a non-autonomous equations.

A common feature shared by both examples is the fact that non-quantum chirality was observed along certain parameter rings [13] in phase diagrams, namely along closed parameter paths in the control space of the oscillators. Along such rings, oscillation stability thrives even in the presence of small parameter fluctuations. The presence of rings in both examples immediately draws attention to the possibility of observing

* Author to whom any correspondence should be addressed.

chiral structures in other complex oscillators displaying rings in the control space.

In hindsight, it is now possible to identify parameter rings in the 'eye of chaos' reported in 2015 for a driven Brusselator [14, 15]. Subsequently, eye of chaos were also observed in a nine-dimensional non-autonomous model of a cracked rotor with oil-film force [16] and, more recently, among the mixed-mode oscillations of a four-dimensional autonomous memristor-based Shinriki's electronic circuit [17]. As illustrated in figure 1, the eye of chaos is a sort of ellipsoidal-like region characterized mainly by chaotic oscillations, surrounded by phases of stable periodic oscillations. In its inner, the phase of chaotic oscillations contains rings of periodic oscillations embedded in them.

The aim of this paper is to report the presence of non-quantum chirality in the self-organization of complex oscillations of the driven Brusselator, as described in section 2. This discovery was only possible thanks to combination of three decisive factors: (i) high-performance computing, (ii) reliable numerical methods and, most importantly, (iii) the use of isospike diagrams, a decade-old technique of representing system stability by counting the number of spikes, i.e. the local maxima, present for every periodic trajectories of the system. This technique is reviewed in section 3. After that, the non-quantum chirality observed in the driven Brusselator is described. Points (i) and (ii) are important because, as discussed in detail below, non-quantum chirality emerges only when plotting phase diagrams like figures 1, 2, and 4 below, which display how the number of spikes of millions of individual oscillators self-organize when pairs of control parameters evolve simultaneously. Such diagrams require relying on fast, efficient and tested numerics [18] over extended parameter intervals, a well-suited task for modern high-performance computer clusters.

2. The driven Brusselator

Complex oscillations in chemical reactions have a long and curious history. Although occasionally reported since at least the early 1800s [19–24], skepticism regarding claims about the existence of chemical oscillations persisted among chemists until well into the 1950s as described, e.g., in the book of Epstein and Pojman [25]. These authors describe the situation citing a 1972 paper of the Danish biochemist Degn [26]: 'although there now seems to be abundant evidence for the existence of homogeneous oscillating reactions, there are still theoreticians who resist the idea, and also a few experimentalists think that alleged homogeneous oscillations are caused by dust particles, although nobody has explained how'.

In pioneering works done in 1910–1920, Lotka [27–31] considered theoretically the problem of chemical oscillations. He was able to derive equations which produced sustained oscillations [31, 32]. However, his equations produced oscillations for any values of the control parameters, something not observed in the chemical laboratory. The damped oscillations predicted by Lotka to be possible in open systems, where a reactant which enters at a constant rate is consumed by an autocatalytic reaction, were observed experimentally by Degn [33]. Lotka's model was subsequently generalized and applied by Selkov and Betz to explain the mechanism of glycolytic self-oscillations [34].

The undriven Brusselator, introduced by Prigogine and co-workers [35, 36], is an important chemical reaction model that was critical to demonstrate the existence of homogeneous oscillations and propagation of waves in chemical reactions. The Brusselator model is interesting in many respects [37]. For his contributions to the study of nonequilibrium systems, Prigogine received the 1977 Nobel Prize in Chemistry [25, 37].

In 1977, Tomita *et al* [38] introduced a forcing term of the form $a\cos(\omega t)$ in the Brusselator, studying the equations

$$\frac{\mathrm{d}X}{\mathrm{d}t} = A - (B+1)X + YX^2 + a\,\cos(\omega t), \tag{1}$$

$$\frac{\mathrm{d}Y}{\mathrm{d}t} = BX - YX^2, \tag{2}$$

where a and ω are freely tunable parameters of the external drive, and A and B are internal parameters. Initially, the main concern was to determine the extension of the regions of entrainment and their stability. The limits of entrainment were estimated with Floquet exponents and compared with results from numerical simulations. In the absence of forcing, limit cycle behavior exists when $B > A^2 + 1$ [39, 40]. The Brusselator is a very useful model to explore dynamics in mass-action kinetic systems. It shows what the possibilities are, e.g., oscillations, excitability, chaos, multistability, pattern-formation, etc.

Among other things, Tomita *et al* [38] reported finding multistability, namely coexistence of two distinct stable oscillations, for $(A, B, a, \omega) = (0.4, 1.2, 0.0018, 0.34)$. Incidentally, multistability as well as the aforementioned eye of chaos were recently rediscovered once again in the Brusselator [41]. Here, following Tomita *et al* [38], we fix $A = 0.4$ and $B = 1.2$ and compute high-resolution phase diagrams displaying how oscillations evolve when tuning the frequency ω and amplitude a of the external drive. For a recent detailed survey regarding the history of the driven Brusselator see the invited review chapter in reference [14], reprinted in reference [15], a book commemorating the 80 years of Prof. Hao Bailin [42].

Before moving on, some words about the origin of the name Brusselator, introduced by Tyson about 50 years ago [39, 40]. I am grateful to him for the following interesting little historical piece [43]:

> 'As a graduate student in chemical physics at the University of Chicago (in 1970), I read the 1968 paper by Prigogine & Lefever in *J. Chem. Phys.*. After referring to it for some months as the 'Prigogine–Lefever' model, I had the idea to start calling it the 'Brusselator', making a rather obvious pun. I introduced the term in my first paper on the subject of chemical oscillations [39].
>
> I was told later that Prigogine, at first, thought this cheeky little grad student was making fun of him, but his colleagues convinced him that it was good publicity for the model. Which it proved to be'.

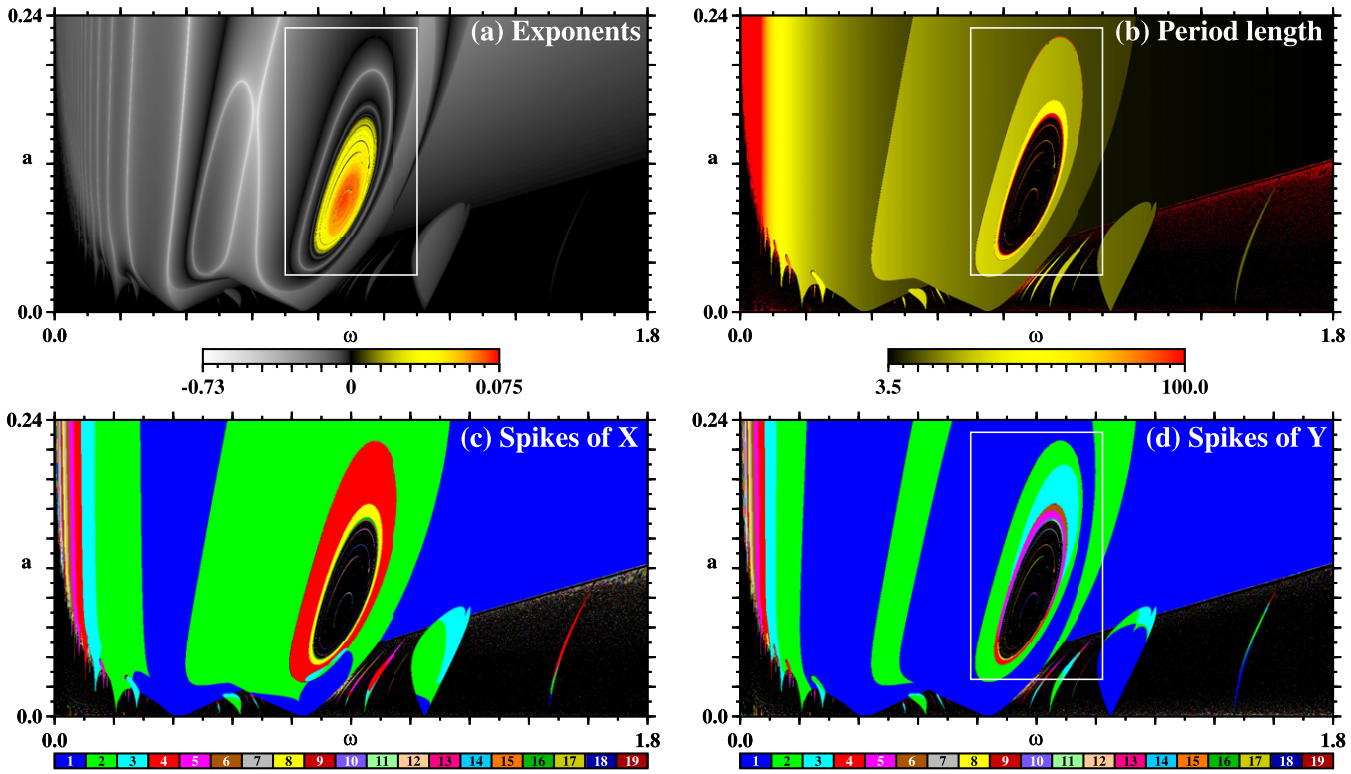

Figure 1. Four distinct ways of representing the nature of stable oscillations of the driven Brusselator. (a) Standard diagram of Lyapunov exponents, with colors representing chaos (positive exponents) and dark shadings representing periodicity (negative exponents). (b) Period length of the oscillations. Black denotes non-periodic oscillations. (c) Isospike diagram showing the number of spikes per period of the X oscillations. (d) Isospike diagram for the Y oscillations. In (c) and (d), black denotes non-periodic oscillations. White boxes mark the eye of chaos [14, 15]. Although (c) and (d) look rather distinct, only the inner spikes distribution depends on the variable used to determine the spikes, not the boundaries between periodic and chaotic oscillations. Individual panels display the analysis of $1200 \times 1200 = 1.44 \times 10^6$ parameter points.

3. The power of counting spikes

The study of regular and irregular trajectories defined by sets of coupled ordinary differential equations essentially amounts to the study of specific quantities associated with the temporal evolution of numerically obtained solutions of the equations. Nowadays, perhaps the most popular tool to explore complex dynamics are the Lyapunov exponents, bounds for the exponential growth rates of the solutions [44]. Lyapunov exponents are essentially mean-field quantities which characterize the rate of separation of the components of initially very close solutions of the equations of motion [45, 46]. For a given set of control parameters, the Lyapunov exponent discriminates regular (negative exponents) and irregular (positive exponents) solutions.

The computation of Lyapunov exponents, topological entropies, and similar quantities derived from solutions of the equations of motion is a rather computer demanding task. Moreover, phase diagrams based on Lyapunov exponents provide no more than just a black-and-white two-color subdivision of the physical control parameter space. But, would it be possible to bypass the expensive computational hurdles while still obtaining reliable two-color diagrams? Or, much better, would it be possible to get more informative phase diagrams with a minimal computational effort? The answer to both questions is affirmative, and the way to do it is to use so-called isospike diagrams [47–57], which we now briefly explain.

The minimal information needed to construct phase diagrams of any type are the solutions of the equations of motion. By simply detecting trajectories that are periodic one may effectively produce black-and-white diagrams of the control parameter space and, therefore, separate periodic from non-periodic trajectories. A simple way to detect if trajectories are periodic or not is by recording the sequence of local maxima, spikes, of the trajectories and then checking if the spikes repeat. Visually, diagrams obtained by discriminating periodic from non-periodic trajectories are basically indistinguishable from analogous diagrams obtained through the expensive calculation of Lyapunov exponents. Lyapunov diagrams are very effective to detect lack of periodicity, while the alternative diagrams based on spikes are very effective to detect periodicity. They both provide divisions into two complementary groups, without discriminating any eventual fine structure of such groups. Clearly, when dealing with periodic oscillations, diagrams based on counting local maxima, spikes, are equivalent to diagrams based on counting local minima.

How to get more informative phase diagrams when detecting periodicity by counting spikes? Here is a simple answer: instead of using just a single color to bunch together all

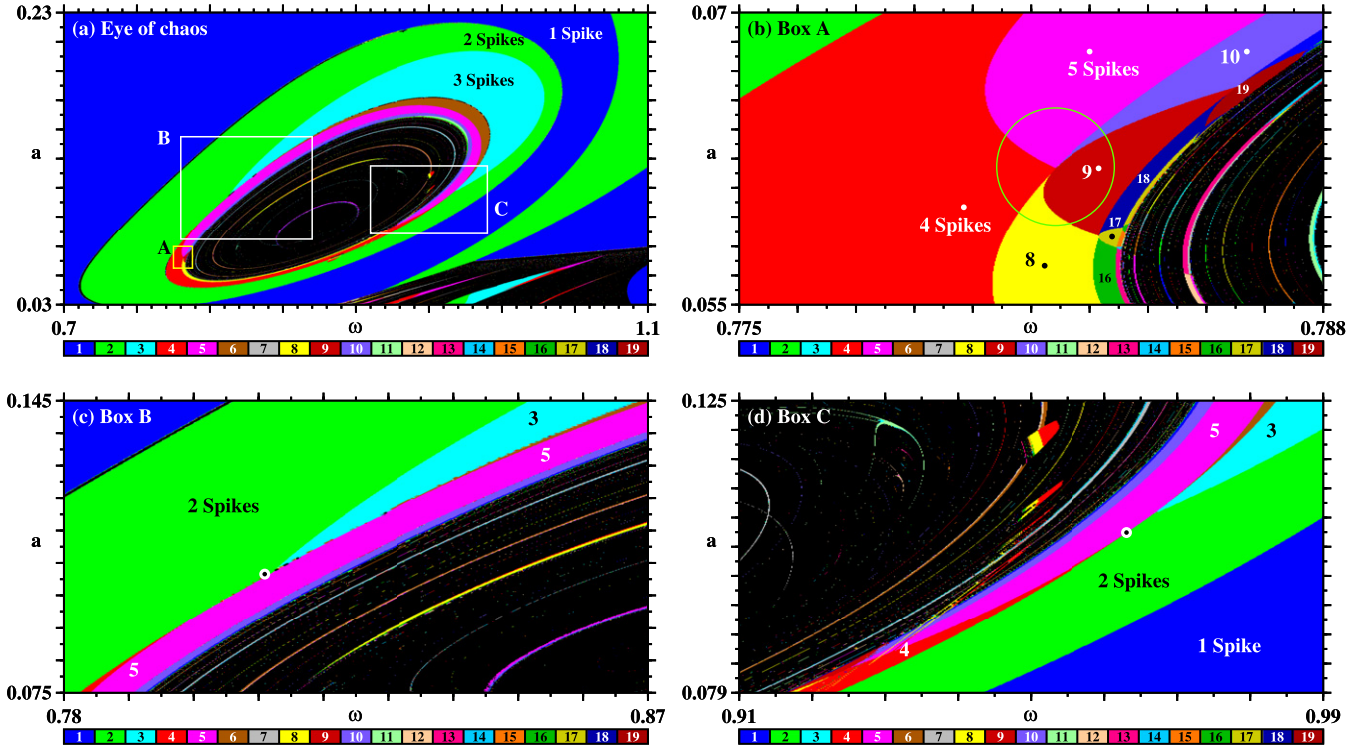

Figure 2. (a) Magnification of box in figure 1(d), illustrating the eye of chaos and chiral structures obtained when counting spikes of Y. Numbers refer to the number of spikes per period of each phase. Boxes A, B and C contain details of the chiral patterns, magnified in the other panels. (b) Magnification of box A in panel (a) showing the 4–5 clockwise oriented chiral pattern. At the circle center there is a quint point [57], where five distinct stability phases meet. The temporal evolutions for parameters indicated by dots are presented in figure 4. (c) Magnification of box B showing a clockwise oriented chiral pattern, with a quint point indicated by the dot. (d) Magnification of box C showing an anticlockwise oriented chiral pattern, with a quint point indicated by the dot. The set of quint points form a lattice [57].

parameters which lead to periodic trajectories, one may use distinct colors to record the specific number of spikes per period of each individual trajectory. Such diagrams are the so-called isospike diagrams [47–57]. Figures 1(c) and (d) provide examples of isospike diagrams, obtained by counting spikes per period of the periodic oscillations of X and Y, respectively. Analogous to what happens for the Lyapunov diagram in figure 1(a) or the diagram based on the period length in figure 1(b), isospike diagrams do not discriminate chaos from quasiperiodicity. Since the number of spikes per period may grow very fast in specific regions of the control parameter space, it is convenient to 'recycle colors' i.e. to plot the number of spikes modulo some convenient integer. For instance, in figures 1(c) and (d) we recycle colors modulo 19.

For each point (ω, a) on the grid we determined whether or not the spikes of X and Y repeated, recording the number of spikes per period for the periodic oscillations, and with black the non-periodic oscillations. In this way we obtain phase diagrams showing parameter domains characterized by oscillations which share the same number of spikes. Such diagrams allow one to visualize directly how the number of spikes evolves when the frequency ω and amplitude a are varied. The phase diagrams in figures 1 and 2 are examples of the diagrams obtained. Clearly, the quality of the final diagrams (and the computational work needed to obtain them) depends of the number of points used in the grids. High resolution diagrams are normally very demanding computational tasks. For a detailed survey on the computation of stability diagrams see reference [55].

Briefly, our isospike stability diagrams are computed as follows. A given $\omega \times a$ window of interest is covered with a mesh of 1200×1200 equidistant points. For each point of the mesh, the temporal evolution of the Brusselator is obtained numerically by solving equations (1) and (2) with a standard fourth-order Runge–Kutta algorithm with fixed time-step 0.001. Integrations are started from an arbitrarily selected initial condition $(x, z) = (0.16, 1.16)$ and proceed by following the attractor [55–57] horizontally from left to right.

4. Results and discussion

Figure 1 shows four diagrams comparing distinct ways of representing the nature of stable oscillations in a frequency-amplitude diagram for the driven Brusselator, equations (1) and (2). This figure compares the classification of the motions using diagrams of Lyapunov exponents, figure 1(a), and period length, figure 1(b), with isospike diagrams for X, figure 1(c), and for Y, figure 1(d). From this figure one clearly sees that the isospike diagrams are much more informative than the other two diagrams. All four diagrams reveal unambiguously the eye of chaos and the associated rings inside and outside the phase defined by chaotic oscillations.

Figures 1(c) and (d) display rather distinct inner distribution and phase boundaries corresponding to periodic oscillations with different number of spikes. In other words, periodic phases look different when inspected by counting spikes with distinct independent variables of the system. However, these differences are similar to the familiar differences observed when attractors are observed in distinct phase-space projections. Manifestly, although the number of spikes per period may differ among distinct variables, the oscillation period measured is always the same, independently of the variable used to determine it.

Figure 2(a) is a magnification of the white box in figure 1(d), showing a more detailed view of the eye of chaos, the black region characterized by non-periodic (chaotic) oscillations. The outer ring of the eye is a domain of parameters characterized by oscillations having one spike per period. Moving farther inward there is a parameter ring of oscillations with two spikes per period. Then, a region with three spikes in the upper right part, and a region with four spikes in the bottom left part. A detailed view of the complex but regular spikes unfolding inside box A is shown in figure 2(b). The three-spikes region gets smaller and smaller as one moves toward smaller values of ω and a, eventually disappearing in specific exceptional points located inside boxes B and C. The two exceptional points were the wedge-like region of three spikes disappears are indicated by black dots in panels (c) and (d). There are many such exceptional points in figure 2(a) and it is easier to understand their meaning by referring to figure 2(b).

The center of the circle in figure 2(b) also contains an analogous exceptional point, a quint point [57] where five distinct stability phases meet. Two phases arise from spikes doublings of phases having four and five spikes. But there is also a parabolic-like phase which arises from spikes adding of two other phases having four and five spikes. All these five phases meet at the center of the circle, the exceptional quint point. Analogously, the points indicated by black dots in figures 2(c) and (d) are also quint points. The five phases meeting in figure 2(c) are the larger and easily visible phases characterized by two, three, and five spikes, as well as by two additional thin wedge-like phases of four and six spikes. In figure 2(c), the five spikes phase is a stretched parabola-like analogous to the nine spikes phase in figure 2(b). Similarly, in figure 2(d) the five phase meeting at the quint point are phases with two, three, four, five, and six spikes.

The most remarkable feature in the panels of figure 2 is the relative orientation of the spikes unfolding. While in figure 2(c) the unfolding proceeds clockwise as $2 \to 3$ and $4 \to 5 \to 6$ etc, in figure 2(d) one sees the opposite situation, namely an anticlockwise unfolding $3 \to 2$, then $6 \to 5 \to 4$, etc.

Figure 3 shows a schematic representation of the first three levels of the clockwise and anticlockwise chiral unfolding seen in figure 2. After a first phase trifurcation, one finds parabolic-shaped phases resulting from oscillations with an odd number of spikes per period, while its adjacent phases have even number of spikes. Clearly, the vertex of each parabola is the meeting point of five distinct phases meet, a quint point [57]. Apparently, the cascading involves just a finite number of steps and

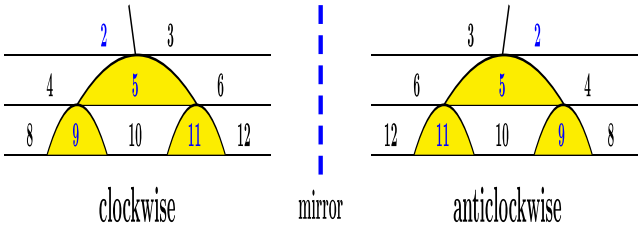

Figure 3. Schematic representation of the first three levels of the clockwise and anticlockwise chiral unfoldings present in figure 2. The cascading has apparently just a finite number of levels and is not very long.

is not particularly long. The two enantiomers seen in figures 2 and 3 form the pair of chiral structures of the Brusselator, and are the main result of this paper. In systems where the cascades forming the enantiomers are found isolated, not forming chiral pairs, the parabolic arcs in figure 3 may overlap [58]. They may also emerge strongly distorted as, for instance, in figure 2.

A minimalist flow particularly suited to investigate the inner details of the cascadings sketched in figure 3 can be obtained by properly linearly shifting variables of a simple quadratic function as follows [59]:

$$\dot{x} = y, \qquad \dot{y} = z, \qquad \dot{z} = -\mathbf{a} - y - \mathbf{b}z + x^2, \qquad (3)$$

where **a** and **b** are freely tunable parameters. The very small number of mathematical operations in equation (3) quite significantly reduces the computational workflow. Theoretical phase diagrams and experimental evidence of quint points and non-quantum chirality for the flow in equation (3) are reported elsewhere [60].

Figure 4 displays the temporal evolution of X and Y for the six representative points indicated in the panels on the top row. The leftmost top panel is shown to contrast the differences observed between spikes of X and Y. As mentioned above, such differences correspond to the familiar differences seen when attractors are projected into distinct phase-space planes. In the six subsequent panels of figure 2, the upper trace shows the time evolution of Y, while the lower trace shows X. The ratios n_X/n_Y refer to the number of spikes found in the X and Y variables, respectively, while T gives the period of the oscillations. Small dots where added to some spikes to help visualize the spikes which belong to a period. Although there are some comparatively small spikes, they are clearly measurable. In particular, note that series with even number of spikes display more subtle variations of the local maxima. For instance, a cursory glance at the panel displaying 16/10 spikes in figure 4 may give the impression of a temporal series having 5 rather than 10 spikes per period, something that closer inspection reveals not to be true.

5. How to experimentally observe non-quantum chirality ?

From the foregoing it is clear what non-quantum chirality is and that there are no means to predict it theoretically, due to

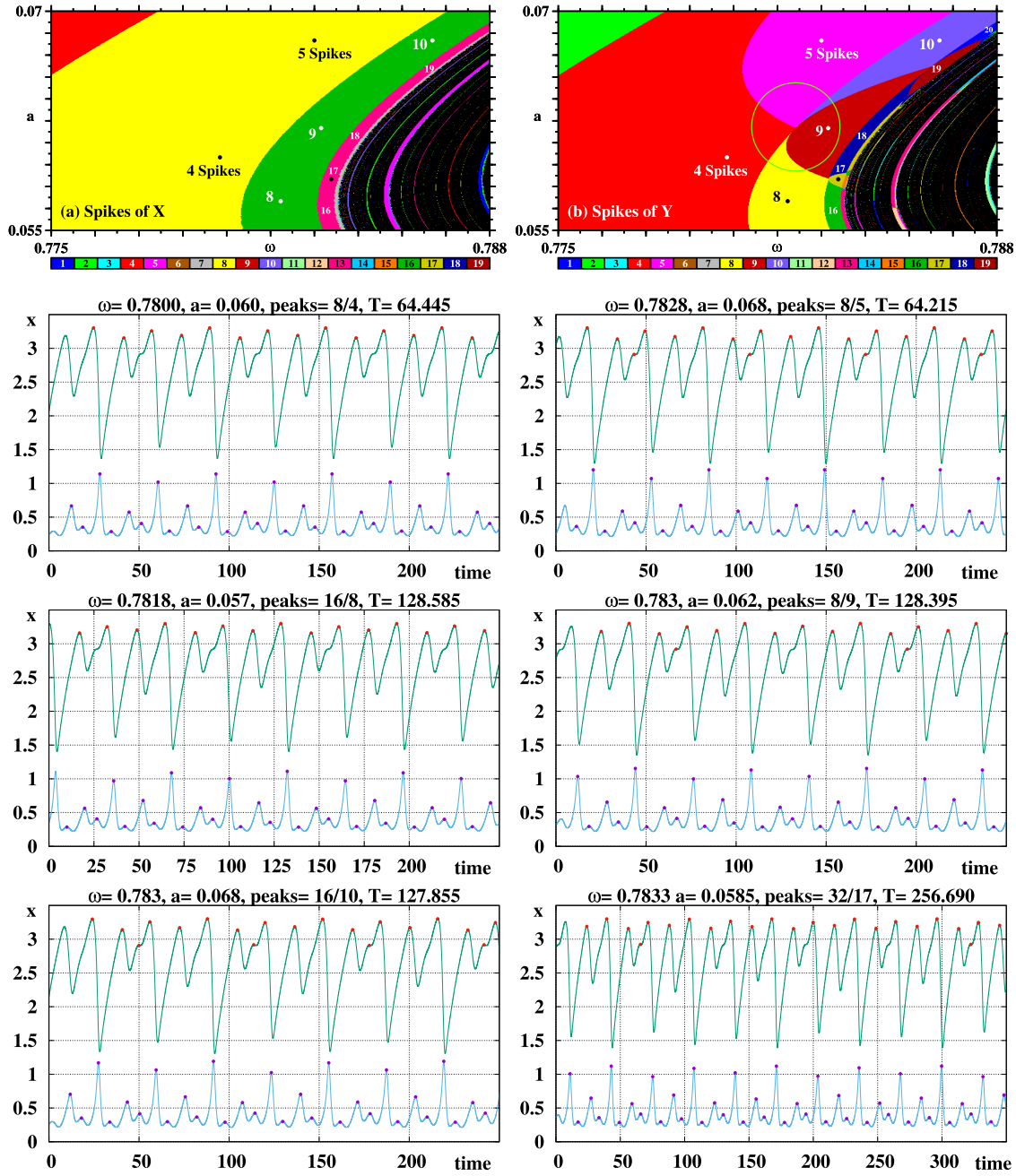

Figure 4. (Top row) Isospike diagrams obtained by counting spikes of X (left panel) and Y (right panel) showing the six points for which the temporal evolution of these variables is illustrated in the subsequent panels. Spikes of X vary in a less complicated way than the spikes of Y. Numbers refer to the number of spikes of some phases. (Subsequent rows) Temporal evolution of X (lower curves) and Y (upper curves). Dots were added to some spikes to help visualization. Numbers n_X/n_Y refer to the number of spikes in each curve, T gives the period of the oscillations. A different temporal window is used in the rightmost panel of the bottom row.

the total absence of analytical methods to solve nonlinear sets of coupled ordinary differential equations. Manifestly, it then becomes important to devise practical methods to effectively measure non-quantum chirality, methods that would work in general, for any system described by arbitrary sets of rate equations of motion.

As illustrated in figure 2, say, patterns defining non-quantum chirality become visible in phase diagrams depicting the variation of the number of spikes for large sets of solutions of the equations of motion and this is the ideal setup for observing them. Such phase diagrams can be obtained experimentally, analogously as already done for an electronic circuit [61]. This is the best method to detect interesting patterns which are formed collectively by large sets of stable periodic solutions of the equations of motion. Although feasible, this methodology is anticipated to be a challenging task in most circumstances, for reasons described in the original work [61].

But such complications may be easily bypassed. Since the temporal evolution of the six points lying inside the phases

indicated in figure 4(b) is known, it suffices to determine the number of spikes for points in these phases, checking then the relative order among adjacent phases, for instance, $4 \to 5$, or $8 \to 9 \to 10$, etc, in figure 4(b). Thus, by simply comparing just a few temporal signals one can identify unambiguously non-quantum chirality. This simpler method was recently used to obtain experimental evidence [60] of quint points and non-quantum chirality for the minimalist flow defined in equation (3) above.

6. Conclusions and outlook

This paper reports the discovery of non-quantum chirality in the frequency versus amplitude control parameter plane of a driven Brusselator, described by equations (1) and (2). These enantiomers mediate families of stable oscillations characterized by different number of spikes (local maxima) per period. The chiral structures reported here are observed through computer simulations because of the complete absence of any framework to obtain analytical solutions for systems of nonlinear sets of coupled differential equations.

Non-quantum chirality is observed by recording how the number of spikes of periodic oscillations evolve when control parameters of the purely classical rate equations of motion are varied. Non-quantum chirality is a not a property of any single trajectory but, instead, arises in specific regions of the control parameter space as a macroscopic collective property due to a large number of distinct trajectories. It is very different from the chirality known to exist among individual orbits of certain algebraic clusters underlying orbital equations of the area-preserving Hénon map, a discrete proxy of open Hamiltonian systems that exhibit chaotic scattering and transport [62].

The decisive feature that allows the observation of non-quantum chirality is the ability to efficiently visualize very large sets of data by using isospike diagrams [47], namely to represent huge sets of stable oscillations in terms of their varying number of spikes per period. As it is clear from the comparisons in figure 1, chirality cannot be found using either the time-honored Lyapunov diagrams, the period length diagrams, or any similar diagrams. Isospike diagrams can be used to analyze arbitrary models governed by sets of ordinary differential equation. Such diagrams are a simple generalization for continuous-time systems of the isoperiodic diagrams used for discrete-time maps [63].

The chirality reported for the Brusselator revises the present knowledge about the topology of the control space this prototypic oscillator, and draws attention to hitherto unsuspected properties of oscillators governed by purely classical (that is, not quantum) equations. So far, all three chiral dynamic systems known involve rings in control parameter space, and it is not clear if this is indeed a necessary condition or just merely circumstantial. In isolation, each of the two structures that compose the chiral pairs were found in diverse systems [51, 58]. The strongly distorted wedge-like phases in figure 2 could be a consequence of having fixed $A = 0.4$ and $B = 1.2$. It would be interesting to check how such phases change when A and B are varied. A puzzling open question is what enforces physical models to be apparently homochiral (to prefer one handedness over the other) and this deserves to be investigated. Lastly, another enticing open question is whether or not it is possible to find chiral dynamic systems governed by maps, not differential equations.

Acknowledgments

This work was partially supported by CNPq, Brazil, grant PQ-305305/2020-4, and by the Max-Planck Institute for the Physics of Complex Systems. All bitmaps were computed at the CESUP-UFRGS Supercomputer Center of the Federal University in Porto Alegre, Brazil.

Data availability statement

All data that support the findings of this study are included within the article (and any supplementary files).

ORCID iDs

Jason A C Gallas https://orcid.org/0000-0003-4378-9083

References

[1] Gallas J A C 2021 Chirality detected in Hartley's electronic oscillator *Eur. Phys. J. Plus* **136** 1048
[2] Kamenetskii E (ed) 2021 *Chirality, Magnetism and Magnetoelectricity* (Berlin: Springer)
[3] Wagnière G H 2007 *On Chirality and the Universal Asymmetry: Reflections on Image and Mirror Image* (Weinheim: Wiley-VCH)
[4] Barron L 2004 *Molecular Light Scattering and Optical Activity* 2nd edn (Cambridge: Cambridge University Press)
[5] Sanganyado E, Lu Z, Fu Q, Schlenk D and Gan J 2017 Chiral pharmaceuticals: a review on their environmental occurrence and fate processes *Water Res.* **124** 527–42
[6] Wade L G Jr and Simek J W 2017 *Organic Chemistry* 9th edn (Harlow: Pearson)
[7] Patterson D, Schnell M and Doyle J M 2013 Enantiomer-specific detection of chiral molecules via microwave spectroscopy *Nature* **497** 475–7
[8] Lobsiger S, Perez C, Evangelisti L, Lehmann K K and Pate B H 2015 Molecular structure and chirality detection by Fourier transform microwave spectroscopy *J. Phys. Chem. Lett.* **6** 196–200
[9] Chen Y-Y, Ye C, Zhang Q and Li Y 2020 Enantio-discrimination via light deflection effect *J. Chem. Phys.* **152** 204305
[10] Kang Y-H, Shi Z-C, Song J and Xia Y 2020 Effective discrimination of chiral molecules in a cavity *Opt. Lett.* **45** 4952–5
[11] Wu J-L, Wang Y, Su S-L, Xia Y, Jiang Y and Song J 2020 Discrimination of enantiomers through quantum interference and quantum Zeno effect *Opt. Express* **28** 33475–89
[12] Gallas J A C 2021 Chirality in a driven ruthenium-catalyzed Belousov–Zhabotinsky reaction model *Phys. Chem. Chem. Phys.* **23** 25720–6
[13] Ramírez-Ávila G M, Kurths J and Gallas J A C 2021 Ubiquity of ring structures in the control space of complex oscillators *Chaos* **31** 101102

[14] Gallas J A C 2017 Periodic oscillations of the forced Brusselator *Peregrinations from Physics to Phylogeny: Essays on the Occasion of Hao Bailin's 80th Birthday* ed K K Phua and M Ge (Singapore: World Scientific)

[15] Gallas J A C 2015 Periodic oscillations of the forced Brusselator *Mod. Phys. Lett.* B **29** 1530018

[16] Rao X B, Chu Y D, Chang Y X, Zhang J G and Tian Y P 20017 Dynamics of a cracked rotor system with oil-film force in parameter space *Nonlinear Dyn.* **88** 2347–57

[17] Rao X-B, Zhao X-P, Gao J-S and Zhang J-G 2021 Self-organization with fast-slow time scale dynamics in a memristor-based Shinriki's circuit *Commun. Nonlinear Sci. Numer. Simul.* **94** 105569

[18] Zeni A R and Gallas J A C 1995 Lyapunov exponents for a Duffing oscillator *Physica* D **89** 71–82

[19] Fechner G T 1828 Über Umkehrungen der Polarität in der einfachen Kette *J. für Chemie und Physik* **53** 128–51

[20] Ostwald W 1896 *Elektrochemie, ihre Geschichte und Lehre* (Leipzig: Veit)

[21] Ostwald W 1900 Periodische Erscheinungen bei der Auflösung des Chroms in Säuren *Z. Phys. Chem.* **35U** 33–76

[22] Ostwald W 1900 Periodische Erscheinungen bei der Auflösung des Chroms in Säuren *Z. Phys. Chem.* **35U** 204–56

[23] Kremann R 1913 *Die periodischen Erscheinungen in der Chemie* (Stuttgart: F. Enke Verlag)

[24] Hedges E S and Myers J E 1926 *The Problem of Physico-Chemical Periodicity* (London: Arnold & Co.)

[25] Epstein I R and Pojman J A 1998 *An Introduction to Nonlinear Chemical Dynamics: Oscillations, Waves, Patterns, and Chaos* (Oxford: Oxford University Press)

[26] Degn H 1972 Oscillating chemical reactions in homogeneous phase *J. Chem. Educ.* **49** 302–7

[27] Lotka A 1910 Zur Theorie der periodischen Reaktionen *Z. Phys. Chem.* **72U** 508–11

[28] Hirniak J 1910 Zur Frage der periodischen Reaktionen *Z. Phys. Chem.* **75U** 675–80

[29] Lotka A J 1910 Contribution to the theory of periodic reactions *J. Phys. Chem.* **14** 271–4

[30] Lotka A J 1912 Ein Fall von Antokatakinese mit oscillatorischem Verlauf *Z. Phys. Chem.* **80U** 159–64

[31] Lotka A J 1920 Undamped oscillations derived from the law of mass action *J. Am. Chem. Soc.* **42** 1595–9

[32] Erneux T 2018 Early models of chemical oscillations failed to provide bounded solutions *Phil. Trans. R. Soc.* A **376** 20170380

[33] Degn H 1973 Chemiluminescence in oscillatory oxidation reactions catalyzed by horseradish peroxidase *Biological and Biochemical Oscillators* ed B Chance, E K Pye, A K Gosh and B Hess (New York: Academic)

[34] Selkov E E and Betz A 1973 On the mechanism of single-frequency glycolytic oscillation *Biological and Biochemical Oscillators* ed B Chance, E K Pye, A K Gosh and B Hess (New York: Academic)

[35] Prigogine I and Balescu R 1956 Phènomènes cycliques dans la thermodynamique des processus irréversibles *Bull. Cl. Sci. Acad. R. Belg.* **42** 256–65

[36] Prigogine I and Lefever R 1968 Symmetry breaking instabilities in dissipative systems. II *J. Chem. Phys.* **48** 1695–700

[37] Nicolis G and Prigogine I 1977 *Self-Organization in Nonequilibrium Systems* (New York: Wiley)

[38] Tomita K, Kai T and Hikami F 1977 Entrainment of a limit cycle by a periodic external excitation *Prog. Theor. Phys.* **57** 1159–77

[39] Tyson J J 1973 Some further studies of nonlinear oscillations in chemical systems *J. Chem. Phys.* **58** 3919–30

[40] Tyson J J and Light J C 1973 Properties of two-component bimolecular and trimolecular chemical reaction systems *J. Chem. Phys.* **59** 4164–73

[41] Rech P C 2021 Multistability in a periodically forced Brusselator *Braz. J. Phys.* **51** 144–7

[42] Sanjuán M A F 2017 *Contemp. Phys.* **58** 298–9 Review of the book in reference [14]

[43] Tyson J J 2021 private E-mail communication

[44] Lyapunov A M 1992 *The General Problem of the Stability of Motion* ed A T Fuller (London: Taylor and Francis) (Engl. transl.)

[45] Pikovsky A and Politi A 2016 *Lyapunov Exponents, A Tool to Explore Complex Dynamics* (Cambridge: Cambridge University Press)

[46] Vallejo J C and Sanjuan M A F 2017 *Predictability of Chaotic Dynamics* 2nd edn (Berlin: Springer)

[47] Freire J G and Gallas J A C 2011 Stern–Brocot trees in the periodicity of mixed-mode oscillations *Phys. Chem. Chem. Phys.* **13** 12191–8

[48] Freire J G and Gallas J A C 2011 *Phys. Lett.* A **375** 1097

[49] Nascimento M A, Gallas J A C and Varela H 2011 Self-organized distribution of periodicity and chaos in an electrochemical oscillator *Phys. Chem. Chem. Phys.* **13** 441

[50] Freire J G, Pöschel T and Gallas J A C 2012 Stern–Brocot trees in spiking and bursting of sigmoidal maps *Europhys. Lett.* **100** 48002

[51] Gallas M R, Gallas M R and Gallas J A C 2014 Distribution of chaos and periodic spikes in a three-cell population model of cancer *Eur. Phys. J. Spec. Top.* **223** 2131–44

[52] Rao X-B, Chu Y-D, Lu-Xu L, Chang Y-X and Zhang J-G 2017 Fractal structures in centrifugal flywheel governor system *Commun. Nonlinear Sci. Numer. Simul.* **50** 330–9

[53] Xu L, Chu Y-D and Yang Q 2020 Novel dynamical Scenario of the two-stage Colpitts oscillator *Chaos Solitons Fractals* **138** 109998

[54] Rodrigues C S, dos Santos C G P, de Miranda R C C, Parma E, Varela H and Nagao R 2020 A numerical investigation of the effect of external resistance and applied potential on the distribution of periodicity and chaos in the anodic dissolution of nickel *Phys. Chem. Chem. Phys.* **22** 21823–34

[55] Gallas J A C 2016 Spiking systematics in some CO_2 laser models *Adv. At., Mol., Opt. Phys.* **65** 127–91

[56] Gallas J A C, Hauser M J B and Olsen L F 2021 Complexity of a peroxidase–oxidase reaction model *Phys. Chem. Chem. Phys.* **23** 1943–55

[57] Field R J, Freire J G and Gallas J A C 2021 Quint points lattice in a driven Belousov–Zhabotinsky reaction model *Chaos* **31** 053124

[58] Gallas J A C 2021 Overlapping adding-doubling spikes cascades in a semiconductor laser proxy *Braz. J. Phys.* **51** 919–26

[59] Gallas J A C 1993 Degenerate routes to chaos *Phys. Rev.* E **48** R4156–9

[60] Volos C K and Gallas J A C 2022 Experimental evidence of quint points and non-quantum chirality in a minimalist autonomous electronic oscillator *Eur. J. Phys. Plus* **137** (accepted)

[61] Sack A, Freire J G, Lindberg E, Pöschel T and Gallas J A C 2013 Discontinuous spirals of stable periodic oscillations *Sci. Rep.* **3** 3350

[62] Endler A and Gallas J A C 2006 Conjugacy classes and chiral doublets in the Hénon Hamiltonian repeller *Phys. Lett.* A **356** 1–7

[63] Gallas J A C 1993 Structure of the parameter space of the Hénon map *Phys. Rev. Lett.* **70** 2714–7